Research article

Synthesis, characterization and optical properties of ZnO-CuO-Al₂O₃ semiconducting films on glass substrates by sol-gel technique

Erdal Çelik[a,b], Funda Öztoprak[b], M. Faruk Ebeoğlugil[c], Işıl Birlik[a], Recep Yiğit[b,d], Metin Tanoğlu[e] and Hasan Aslan[f]*

[a]Department of Metallurgical and Materials Engineering, Dokuz Eylul University, Izmir, Turkey
[b]Center for Fabrication and Application of Electronic Materials, Dokuz Eylul University, Izmir, Turkey
[c]Department of Ceramic Engineering, Dumlupınar University, Kutahya, Turkey
[d]Department of Technical Programs, Izmir Vocational School, Dokuz Eylul University, Izmir, Turkey
[e]Department of Mechanical Engineering, Faculty of Engineering, Izmir Institute of Technology, Izmir, Turkey
[f]Department of Physics, Faculty of Science, Gebze Institute of Technology, Gebze, Turkey

Abstract

We systematically report synthesis, characterization and optical properties of ZnO-CuO-Al₂O₃ semiconducting thin films on glass substrates in terms of preparation condition such as Cu content for gas sensor applications. In this framework, the thin films were successfully fabricated by sol-gel dip-coating technique using Zn, Cu and Al based precursors as starting materials. Transparent solutions were prepared by dissolving the Zn acetate, Cu and Al chlorides in solutions of methanol and glacial acetic acid. Turbidity, pH values, wettability and rheological properties of the prepared solutions were measured by turbidimeter, pH meter, contact angle ganiometer and rheometer machines before coating process. Turbidity, pH and contact angle values of the solutions were found to be approximately 34 ntu, 4.5 and 18°, respectively. It was determined that viscosities of the solutions slightly changed with increasing Cu concentration. The measured gel points of ZnO-0, 5, 10 and 15% CuO-Al₂O₃ solutions were approximately determined as 4000, 3500, 3000 and 2500 sec, respectively. The ZnO-CuO-1 wt% Al₂O₃ composite films with 0, 5, 10 and 15 wt% CuO content were obtained on glass substrate by dipping and the gel films were dried at 300°C for 10 min and followed by heat treating at 500°C for 10 min in air. This process was repeated six cyclics to make thick films. The thick films were annealed at 600°C for 30 min in air. The thermal, structural, microstructural, adhesion and optical properties of the coatings were extensively characterized by using DTA-TG, FTIR, XRD, SEM-EDS, AFM, scratch tester, refractometer and spectrophotometer. The annealing temperature, 600°C, can completely remove all templates from Zn, Cu and Al networks and oxide crystalline structure is completely formed at this temperature. The spectrum of ZnO-CuO-Al₂O₃ precursor film heat-treated at 500°C and 600°C which shows an absence of absorption bands corresponding to organics and hydroxyls indicating complete removal of organics and hydroxyls. XRD study confirms that the composite films consist of ZnO and CuO phases after annealing process. SEM reveals that dense structures are obtained by increasing CuO content in the composite films. It is clear from EDS analysis that Zn, Cu and Al elements are present in the films and Al peak is very low because it has 1% Al₂O₃ in the films. It was found that surface roughnesses of the films changed between 90 and 200 nm. The films prepared from 15% CuO have better adhesion strength to the glass substrate among other coatings. Refractive indices of ZnO based sol–gel coatings usually lie within the interval 1.20–1.70. While pure ZnO films has a high porosity, the porosity values of ZnO-5, 10 and 15% CuO-Al₂O₃ films decrease as a function of CuO content. The film thicknesses for ZnO-0, 5, 10 and 15% CuO-Al₂O₃ were measured as 852

---

*Corresponding author: Tel: +90 – 232 – 4127459, Fax: +90 – 232 – 4127452
e-mail: erdal.celik@deu.edu.tr

nm, 478 nm, 518 nm and 695 nm using optical method respectively. The optical direct band gap energies were found to be in the range of 3.18 to 3.15 eV for ZnO-CuO-1 wt% Al_2O_3 films including 0, 5, 10 and 15 wt% CuO content. The ZnO film shows the transmittance of the order of 44% while that of ZnO-CuO-Al_2O_3 films was of the order of 55%. It is noticed that the ZnO film has higher absorbance in visible range of spectrum.

Keywords: *ZnO-CuO-Al_2O_3 films, sol-gel, semiconductivity, adhesion, optical direct band gap*

---

1. Introduction

Now that zinc oxide (ZnO) films are n-type wide-gap semiconductors (3.3 eV) with optical transparency in the visible range and it is possible to dope them conveniently, ZnO films have been targeted as useful materials for developments of electronic and optoelectronic devices such as transparent conductors, solar cell windows, gas sensors, and surface acoustic wave devices [1-3]. As a gas sensor material, ZnO is used to detect reducing gases such as CO and H_2 [4]. In order to improve the sensitivity and selectivity, Pd and Au are added on the surface of the sensor as additive materials. Besides, the sensors are made in thick and thin films. Ever since the possibility of the CO gas selectivity of p–n heterocontact sensors has been reported, the various forms of the heterocontact sensors are also being tested, including mechanical contact type, thin film type, and composite form [5,6].

Gas sensors that include semiconducting metal-oxides such as ZnO are found to be very useful for detecting the toxic gases. The fundamental sensing principle relies on the change of conductivity of the sensors when they are exposed to certain target gases at moderate temperatures. Notwithstanding the fact that the mechanism of the gas sensing is rather complicated [2], it is believed that the decrease in resistivity in n-type semiconductor gas sensors as exposed to reducing gases results from the desorption of oxygen absorbed on the surface and grain boundaries of metal-oxides at high temperatures in air. One of the demands on the gas sensors is the low power consumption. A low resistance material provides the lower driving power once it is used as a sensor [7].

Composites of n-type ZnO are expected to show the reduced sensitivity due to their opposite response to reducing gases, however, they show good CO gas sensitivity with the controlled addition of Al. The Al doping into CuO is shown to reduce the electrical conductivity of CuO and the reduced conductivity of CuO is proposed to be responsible for the increase of the CO gas sensitivity of ZnO–CuO composite by increasing the current through p–n junction. It was also demonstrated that the conductivity is controlled by ZnO–CuO boundaries [5,6]. In addition, Al_2O_3 doped ZnO thin films are characterized as a wide band gap semiconductor. It has an application such as gas sensors due to its low conduction as compared to the single component oxide of ZnO and a lower power requirement is needed for them. Co-addition of CuO and Al_2O_3 develops p-type conduction by reducing gas sensitivity of ZnO film. Al_2O_3 is shown to reduce the electrical conductivity of CuO and the reduced conductivity of CuO is proposed to be responsible for the increase of the CO gas sensitivity of ZnO-CuO-Al_2O_3 composite by increasing the current through p-n junction. Conductivity is controlled by ZnO-CuO boundaries [8,9]. With regard of ZnO thin film with doping metal oxides, there are a few reports in the literature, especially consisting of three ZnO, CuO and Al_2O_3.

ZnO-based thin films can be deposited by a number of different techniques like radio-frequency magnetron sputtering, dc and ion beam sputtering [7], reactive evaporation, spray pyrolysis [8], metalorganic chemical vapor deposition (MOCVD) [10] and sol–gel [11]. As one of the alternative approaches, sol–gel technique has drawn much interest in preparing thin layer ceramic materials from a liquid precursor solution and also has several advantages in producing thin films suitable for the gas sensor, such as inexpensive, simple facilities relatively homogeneous composition, easy control of film thickness and fine and porous microstructure [4,11,12]. In addition to these advantages of the sol-gel process, the thin films can be prepared on a large surface and long-length tapes [11]. The films with preferential c-axis orientation can be easily obtained even on glass substrates. In the sol-gel process, oxide films are obtained by post-deposition crystallization. As-deposited films are amorphous states and must be transformed into crystalline states by post-annealing. There are many factors the crystallization behavior of the films such as substrates used, solution chemistry (structure of sols and chemical and thermal stability of organic compounds involved), heat treatment conditions (temperature, heating rate and atmosphere) and so on. When the sol-gel derived as-deposited films are annealed, the resultant oxide films generally exhibit random orientation of crystalline grains because of nucleation and crystal growth in bulk of films [13].

In the present paper, we emphasized on a detailed account of characterization and optical properties of ZnO-CuO-Al$_2$O$_3$ semiconducting thin films on glass substrate synthesized by sol-gel dip-coating technique using solutions of Zn, Cu and Al based precursors, solvent and chelating agent. This research serves six main purposes: (a) solution characteristics, (b) determination of heat treatment regimes, (c) structural features (d) surface properties, (e) adhesion and (f) optical behavior. According to this aim, turbidity, pH measurement, wettability and rheological properties of the prepared solutions were determined since solution preparation and processing have a large influence on final properties of films. In this context, the present contribution is devoted to optimization of the preparation by sol-gel of ZnO-CuO-Al$_2$O$_3$ films with different CuO contents. In order to define chemical structure and reaction type of intermediate temperature products and to use suitable process regime, Differential Thermal Analysis-Thermogravimetry (DTA-TG) and Fourier Transform Infrared (FTIR) devices were used in the film production. Structural analysis of the produced films was performed by using multipurpose X-Ray Diffraction (XRD) and surface morphology was investigated using Scanning Electron Microscopy-Energy Dispersive Spectroscopy (SEM-EDS) and Atomic Force Microscopy (AFM). Adhesion properties of ZnO-CuO-Al$_2$O$_3$ composite films were determined by scratch tester. Optical properties of the produced films were investigated using refractometer and spectrophotometer devices.

2. Experiment Procedure

2.1. Solution Preparation

The sol–gel films were obtained by simplified sol–gel method using metal based precursors. For this process, zinc acetate dihydrade (Zn(CH$_3$COO)$_2$.2H$_2$O), copper chloride (CuCl$_2$) and aluminum chloride (AlCl$_3$.H$_2$O) precursors (High Pure Material tri Chemical Laboratory) were used as received. The precursors were weighted out in fume hood and the solutions were then prepared using Zn, Cu and Al alkoxides or salts, solvent and chelating agent. Precursor materials were dissolved in 40 ml of methanol in separate 250 ml round-bottomed flasks for a thorough atomic-scale mixing. Glacial acetic acid was then added into the prepared solutions as chelating agent. The resultant solutions were

mixed and refluxed at room temperature for 60 min in order to yield clear and homogeneous solutions (see Fig. 1 for details). The stability of the process is set by control of the hydrolysis and condensation reactions such they take place only when the solutions dries, solvent is lost or temperature is elevated.

In order to much better understand solution characteristics which affect thin film structure, turbidity, pH values, wettability and rheological properties of the prepared solutions were respectively measured by turbidimeter, pH meter, contact angle measurement and rheometer machines before coating process. Turbidity properties of the solutions were measured to use standard solutions for coating process by VELP TB1 Model turbidimeter. Measurement range was taken in the range of 0 and 1000 ntu (nephelometric turbidity unit). After preparation of transparent solutions, pH values of the solutions were measured to determine their acidic and basis characteristics using a standard pH meter with Mettler Tolede electrode. Wettability properties of the solutions were determined by measuring their contact angle (θ) using KSV Glass 100 Instrument contact angle machine. In addition to pH value, wettability and turbidity properties, rheological behaviour of the solutions including viscosity, gel point, shear stress, viscous and elastic moduli was scrutinized by CVO 100 Digital Rheometer (Bohlin Instrument).

2.2. Coating Process

Prior to the coating process, glass substrates with dimension of 15 mm x 15 mm x 3 mm were cleaned in acetone. The solutions were deposited onto the glass substrates by using dip-coating technique at room temperature. The solutions were deposited on the substrates by using a dip coating process with a withdrawal speed of 0.3 cm/sec and with staying within the solution for 3 min. The temperature of solutions was kept at room temperature in our laboratory. As demonstrated in Ref. [14], the dip coating involves the formation of a film through a liquid entrainment process that may be either batch or continuous in nature. The general steps include immersion of the substrate into the dip-coating solution, start-up, where withdrawal of the substrate from the solution begins, film deposition, solvent evaporation, and continued drainage as the substrate is completely removed from the liquid bath. The film thickness formed in dip coating is mainly governed by viscous drag, gravitational forces, and the surface tension. The as-coated gel films were dried at 300°C for 10 min and subsequently heat-treated in an electrical furnace at 500°C for 10 min in air. This heat treatment decomposed the precursor film and oxidized it so as to produce ZnO-CuO-Al_2O_3 composite films. We repeated 6 times of this film-making process. The thick multilayered ZnO-CuO-Al_2O_3 films were annealed at 600°C for 30 min in an electrically heated tube furnace to make them polycrystalline. The compositions of the obtained ZnO-CuO-1 wt% Al_2O_3 films were 0, 5, 10 and 15 wt% CuO. The content of Al_2O_3 was held in a constant value. Nonetheless, the content of ZnO was changed depending on CuO. Fig. 1 shows the flow diagram for ZnO-CuO-Al_2O_3 semiconducting thin films prepared sol-gel process using dip-coating method.

Zn, Cu, Al precursors

Dissolve with acetic acid

Dilute with methanol

Mixing (25°C for 1 h in air)

Transparent solution

Dipping

Drying
(300°C, 10 min, air)

Repeat

Heat treatment
(500°C, 10 min, air)

Annealing
(600°C, 30 min, air)
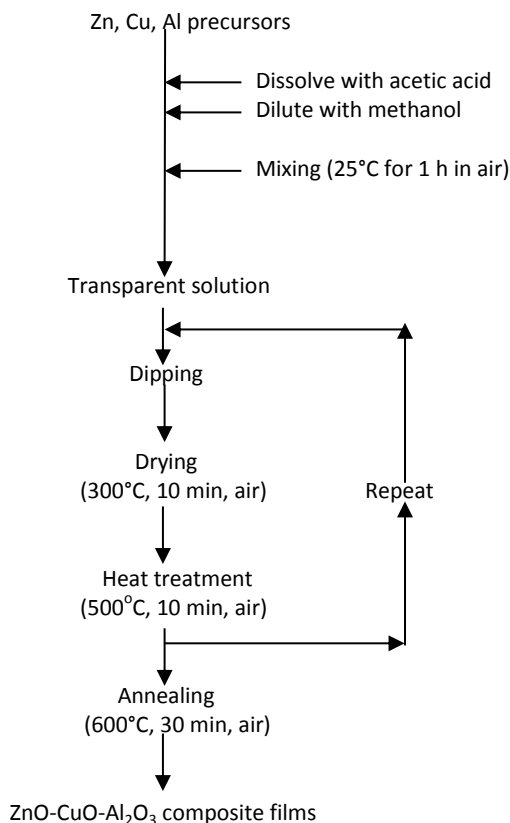
ZnO-CuO-Al$_2$O$_3$ composite films

Fig. 1 Processing steps of sol-gel dip-coating technique

2.3. Characterization

Thermal behaviors of Zn, Cu and Al-based powders, which were dried at 150°C for 0.5 hours in air, were evaluated to gain decomposition and phase formation at a heating rate of 10°C/min under oxygen atmosphere by using DTA/TG machine (DTG-60H Shimadzu). Al$_2$O$_3$ powder was used as a reference material. The enthalpies of solvent removal and combustion were obtained using TA 60WS Software of Shimadzu 60AH. This software derived the enthalpies by calculation of total area under each peak with respect to the base line from start to end temperature. FTIR (Perkin Elmer) absorption spectra were measured over the range of 4000 to 400 cm^{-1} at room temperature after the reactions in the temperature range of 25°C and 600°C for 30 minutes in air. After preparing powders at these temperatures, they were mixed with potassium bromide KBr. All of these five samples were characterized by FTIR. % Transmittance-wavelength and % Absorbance-wavelength curve can be obtained. According to the results, depending on temperature, variation of organic component's concentration can be determined by Fluka library supplied by Perkin-Elmer.

XRD patterns of thin films were determined to identify phase structure by means of a Rigaku (D/MAX-2200/PC) diffractometer with a CuK$_\alpha$ irradiation (wavelength,

λ=0.15418 nm) by both θ-2θ mode and 2θ scan mode. Thin-film XRD geometry where incident angle was fixed at 1° was used to collect data from only thin films. The surface topographies and elemental analysis of ZnO-CuO-Al₂O₃ films were examined by using a JEOL JJM 6060 SEM attached with EDS. Surface roughness of ZnO-CuO-Al₂O₃ semiconducting thin films on glass substrate was characterized by an atomic force microscope (AFM) with model, Nanopics 1000 (NPX 100). AFM data, collected by Tapping Mode imaging using a silicon tip with a radius of curvature less than 5 nm, were computed from spectral analysis. AFM images were acquired using the intermittent contact mode at a scanning frequency of 1 Hz. Intermittent contact mode, or 'tapping' mode, is preferred over contact mode for surface roughness measurements with the AFM. The AFM measurements were performed in air. These silicon cantilevers support a ∼6 μm long, 12° conical AFM tip with a 10 nm radius of curvature.

Adhesion properties of ZnO-CuO-Al₂O₃ films were determined by SHIMADZU Scanning Scratch Tester (SST-W101 Model). Scratch test is carried out to determine and analyze the adhesion strength of a coating to a substrate. In the test, a diamond stylus scratched over the coated surface with a constant speed under progressing normal load until a critical force is reached, at which adhesion failure is detected. This critical load is used as a measurement of the adhesion between coating and substrate. In this study, adhesion strength of coatings was evaluated by using a scanning scratch tester with a 15 μm tip radius diamond stylus. The applied load was 98 mN for all samples. During the test, a stylus was drawn on coating surface with a sliding speed of 5 μm.s^{-1} keeping scanning amplitude of 10 μm which perpendicular to the scratching direction at the same time. Load was carried out progressively to the stylus with a loading speed of 2 μm.s^{-1}. Friction on the stylus increases with increasing load, which causes a delay in movement between cartridge body and stylus. This delay is defined as a cartridge output.

Optical properties of the produced ZnO-CuO-Al₂O₃ films were evaluated using refractometer and spectrophotometer machines. Refractive indexes of thin films were measured at selected wavelengths in the VIS region by a high-accuracy Abbe refractometer at room temperature. Refractive indexes were used to determine film thickness, porosity and optical band gap values using V-530 JASCO UV/VIS Spectrophotometer. Porosity of films can be calculated using refractive index as reported in a research of A. Diaz-Parralejo et al. [15]. Notably, direct evaluation of thin film porosity is not easy. To the best of our knowledge there are three expressions in the literature for evaluating porosity in terms of the refractive index of the film. The simplest is:

$$P = \frac{n - n_d}{1 - n_d} \tag{1}$$

where P is the pore volume fraction, n the refractive index of the porous film, and n_d the refractive index of the film after full densification performed by using annealing process at 600℃. A modification of Eq. 1 has been proposed in the form (Ref. [15] and references therein):

$$P = \frac{n - n_d}{1 - n_d}\frac{n + n_d}{1 + n_d} = 1 - \frac{n^2 - 1}{n_d^2 - 1} \tag{2}$$

which is frequently reported in the literature. Finally, another widely accepted expression for *P* is:

$$P = 1 - \left(\frac{n^2 - 1}{n_d^2 - 1} \right) \left(\frac{n_d^2 + 2}{n^2 + 2} \right) \tag{3}$$

which is derived from the Lorentz–Lorenz expression [15].

Regarding optical band gap of $ZnO-CuO-Al_2O_3$ films on glass substrates, it is well known that in an amorphous material like glass characterized by indirect allowed transitions, the absorption coefficient varies with the photons energy according to the Tauc's relation [16]:

$$\sqrt{\alpha h \nu} = B(h\nu - E_{opt}) \tag{4}$$

where ν is the frequency of incident photons, E_{opt} the optical gap, *h* the Planck's constant and *B* a constant. The variation of $(\alpha h\nu)^{1/2}$ as a function of the energy *hν* shows a linear behavior near the band gap. The value of the energy band gap is given by the intercept of the straight line with the energy axis. In addition to these, transmittance and absorbance properties of $ZnO-CuO-Al_2O_3$ thin films on glass substrate by V-530 JASCO UV/VIS Spectrophotometer with a blank piece of substrate in the reference beam.

3. Results and Discussion

3.1. Solution Characteristics

The sol–gel process can generally be divided into the following stages: forming a solution, gelation, drying, heat treatment, annealing and so on. The key to synthesizing thin films through this route lies in the formation of solutions and gels of high quality. Also, optimum structural, thermal, microstructural optical and gas sensitivity properties are directly related to solution characteristics such as turbidity, pH, wettability and rheology because they present an important clue for further processing. At the first step of these kinds of researches, some main problems like dissolubility and gelation/precipitation are encountered. These problems strongly depend on turbidity, pH, wettability and rheology of the solutions.

3.1.1. Turbidity

Turbidity which means the relative cloudiness of a liquid gives the optical characteristic of suspense particles in a liquid. Light is passed through the sample and is scattered in all directions. The light that is scattered at 90° angle to the incident light is then detected by a photo diode and is converted into a signal linearized by analyzer and displayed as ntu. The more suspended particles there are in a liquid, the more light will be scattered, resulting in a higher ntu value [17].

With turbidity experiments, whether solutions are dissolved very well is understood as ntu values before coating process. As stated before, the measurement range is between 0 ntu and 1000 ntu. It is interpreted that powder based precursors is completely dissolved as turbidity value approaches to 0 ntu and they are not dissolved and some powder particles are suspended in a solution as it approaches to 1000 ntu. The fabrication of

homogeneous, continuous and thin film depends directly on turbidity value which is 0 ntu. Here turbidity tests were evaluated using Cu concentration in the solutions. Turbidity values of the prepared solutions are listed in Table 1. Turbidity values of the $ZnO-CuO-Al_2O_3$ solutions including 0, 5, 10 and 15% CuO were measured as 33.90, 33.70, 34.80 and 33.80 ntu, respectively. This effect of Cu concentration was not also quite dependent on the ratio on account of the fact that the solutions had almost the turbidity values. Turbidity was slightly affected by Cu concentration in the solution. Furthermore, there is somewhat scatter in the results but the trends remains almost the same values which mean low turbidity, indicating that the solutions are clear and transparent at room temperature.

Table 1

Turbidity values of the solutions

Solutions	Turbidity (ntu)
ZnO	33.90
$ZnO-5\%CuO-Al_2O_3$	33.70
$ZnO-10\%CuO-Al_2O_3$	34.80
$ZnO-15\%CuO-Al_2O_3$	33.80

However, after being heated to a certain temperature near the sol–gel transition temperature, the transparent solution starts to become turbid, followed by the sharp increase turbidity values. The solutions samples become completely opaque within a narrow temperature range, and cloudy and solidified gel is formed. The behavior is remarkably similar to the results presented by Y. Xu et al. [18]. The increase in turbidity is believed to be due to the formation of large clusters or aggregates and eventually a gel network structure during heating, which leads to the strong light scattering. It should be true that the denser a gel network formed, the higher the turbidity value is. Gelation has been extensively characterized by measuring clouding point using the turbidity values, but in this study we were only interested in preparation of transparent solutions and it will be explained it in rheological properties later. Based on these results, it can also be pointed out that powder based precursors are dissolved in the solutions. It is striking that films prepared from completely undissolved solutions are not homogeneous, continuous and thin. As a result of this, optimum structural, thermal, microstructural optical and gas sensitivity properties are not obtained by using undissolved solutions.

3.1.2. Acidic Characteristics

The sol–gel process involves the hydrolysis of an alkoxide or salt precursors under acidic or basic conditions, followed by polycondensation of the hydroxylated monomers to form a porous gel network. Afterwards, gel aging and drying can be conducted in order to obtain densified solid matrices. The rate, extent and even the mechanism of the reaction are profoundly affected and may be controlled by many factors such as pH, water:alkoxyde ratio (R), type of catalyst, solvent and precursor, as previously noted by P.C.A. Jerónimo et al. [19]. The pH value of solutions strongly depends on these factors. In our case, we exclusively found that the functional dependence is essentially identical to that seen at these applications, showing that transparent solutions were obtained by preparing with weak acidic conditions thereby concentrations of solvent and chelating agent was remained at a constant concentration but Cu content was increased in the solution. The pH values of the solutions were found to be in the range of 4.28 and 4.59 as

shown in Fig. 2. The pH value of the solution slightly decreased as a function of Cu content in the solution. In spite of the fact that the pH value of pure Zn based solution was especially 4.28 on account of no Al precursor, the higher pH values were obtained depending on $CuCl_2$ concentration. Nevertheless, the interesting point is that the pH values decreased depending on $CuCl_2$ concentration because Cl content, which comes from Cu- and Al-based chlorides, increased in the solutions. In agreement with the results obtained with a research of M. Sheffer et al. [20], it can be noted that the pH changes accelerate the condensation process, i.e., the polymerization, resulting in the deposition of an insoluble film on substrate.
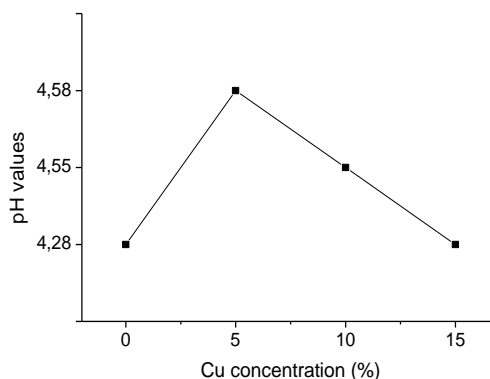
Fig. 2 The pH values of the solutions

It is worth mentioning that their pH value is a significant issue to determine transparent solutions. Inasmuch as pH value of the solution is an important factor influencing the formation of the polymeric three-dimensional structure of the gel during the gelation process, it should be taken into consideration while preparing solutions. While ramified structure is randomly formed in acidic conditions, separated clusters are formed from the solutions showing basic characters. On the other hand, in acidic condition, the formation and aggregation of primary particles occur together and that ripening contributes little to growth after the particles exceed 2 nm in diameter. Developing gel networks are composed of exceedingly small primary particles. In basic condition, the clusters (2–4 nm in diameter) are formerly aggregated by the primary particles and these clusters are later linked to form the gel networks [21]. The other factor is dilution of the solution using solvent. The excess solvent physically affects the structure of the gel, because the liquid phase during the aging procedures mainly consists of the excess solvent. The changes in the gel structure at this stage partly influence the structure of the final film [22].

3.1.3. Wettability

In order to determine wettability properties of the prepared solutions, their contact angles were measured as a function of Cu concentration in the solutions. Wettability properties of the solutions give an important clue for further processes in the sol-gel technique about how to produce crack-free, pinhole-free, continuous and textured films before starting film fabrication. The properties of spreading liquid on substrate present film quality. As demonstrated in Ref. [23], as liquid solution evaporates from the gel at room temperature, the network of the gel becomes and then a solid–vapor interface appears. This raises the energy of the system, because if solid–vapor interfacial energy (γ_{SV}) is bigger than solid–liquid interfacial energy (γ_{SL}), that is $\gamma_{SV} > \gamma_{SL}$, so liquid tends to flow from the interior of the gel to the cover exposed solid. As it stretches toward the

exterior, the liquid goes into tension, and this has two consequences: (1) liquid tends to flow from interior along the pressure gradient; and (2) the tension is balanced by compressive stress in the network that causes shrinkage. On the other hand, the driving forces for shrinkage during drying of the gel coatings include stresses produced by the chemical reactions, as well as osmotic, disjoining and capillary forces. During the drying process, these stresses cause to cracks in thick films. Moreover, the balance of the tensions at the point of intersection leads to a relationship between the surface tensions. This is known as Young's equation [23]:

$$\gamma_{SV} = \gamma_{SL} + \gamma_{LV} \cos \theta \tag{5}$$

If θ=0, the liquid is said to be a spreading liquid, and the solid will be covered with a liquid film. When θ=0, crack-free films are produced owing to very thin gels on the substrate. However, if θ>0, the solution liquid does not spread on the substrate. In that case, thick gel films take place on the surface of the substrate and thus cracking occurs. In our experiments, the contact angles for the ZnO-CuO-Al$_2$O$_3$ solutions including 0, 5, 10 and 15% CuO were found to 18.01°, 16.01°, 17.02° and 21.38°, respectively. Since the contact angles of the solutions approaches to 0° as given in Fig. 3, these results are reasonable before coating process. Surface morphologies of the films strongly vary with the sol nature influencing wettability, but in this study, all solutions were in the same character except Cu concentration. A variation in the contact angles will be a result of Cu content. Regardless of the contact angle of pure Zn-based solution, 18.01°, the contact angle slightly increases when increasing the Cu concentration in the solution, reaching a value around 21.38°. These small variations were elucidated as a function of Cu concentration. The effect of this observation can be confirmed from microstructure of the film, as will be mentioned later.
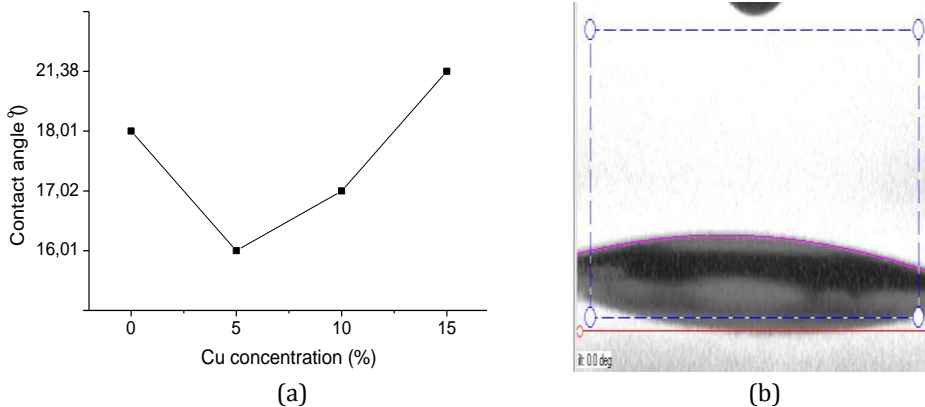
Fig. 3 (a) Contact angle values of the solutions and (b) contact angle position of the ZnO-10% CuO-1% Al$_2$O$_3$ precursor solution

3.1.4. Rheological Properties

Gelation occurs when aggregation of particles or molecules takes place in a liquid, under the action of van der Waals forces or via the formation of covalent or noncovalent bonds [24]. The simplest picture of gelation is that clusters grow by condensation of polymers or aggregation of particles until the clusters collides; then links form between the clusters to produce a single giant cluster that is called a gel. The giant spanning cluster reaches

across the vessel that contains it, so the sol does not pour when the vessel is tipped. At the moment that the gel forms, many clusters will be present in the sol phase, entangled in but not attached to the spanning cluster; with time, they progressively become connected to the network and the stiffness of the gel will increase. According to this picture, the gel appears when the last link is formed between two large clusters to create spanning cluster. This bond is no different from innumerable others that form before and after the gel point, except that it is responsible for the onset of elasticity by creating a continuous solid network. As one would expect from such a process, no latent heat is evolved at the gel point, but the viscosity rises abruptly and elastic response to stress appears [25,26].

The process can be investigated using rheological measurement techniques. The sudden change in rheological behavior [26] is generally used to identify the gel point in a crude way. For example, the time of gelation (gel point) which characterizes the transition from liquid to solid state, is sometimes defined as corresponding to a certain value of viscosity, η; alternatively, it may be defined as the point where the gel shows so much elasticity that the probe (e.g., rotating spindle) tears the gel. The problem with this approach is that the rate of increase of the viscosity varies with the preparation conditions, so that a particular value of viscosity (say, 1000 Pa.s) might be observed seconds before gel point in one system, but hours before gel point in another. A more elegant and informative way to look at gelation is to measure the viscoelastic behavior of the gel as a function of shear rate [25-27].

Table 2
Rheological properties of the solutions at 30°C

Solutions	Viscosity (mPa.s)	Shear stress (Pa)	Viscous modulus (Pa)	Elastic modulus (Pa)	Gel point (sec)
ZnO	1.21	0.364	0.199	1.880	4000
ZnO-5%CuO-Al$_2$O$_3$	1.42	0.363	0.146	1.750	3500
ZnO-10%CuO-Al$_2$O$_3$	1.35	0.384	2.840	0.929	3000
ZnO-15%CuO-Al$_2$O$_3$	1.23	0.368	0.102	1.830	2500

This evaluation is extremely important, since the microstructure and therefore the optical properties of the film are obtained in this part of the process. Table 2 shows rheological properties such as viscosity, gel point, shear stress, viscous and elastic moduli for the prepared solutions as a function of Cu concentration in details. The relative viscosity values of the obtained ZnO-CuO-Al$_2$O$_3$ solutions having 0, 5, 10 and 15% CuO were found to be 1.21 mPa.s, 1.42 mPa.s, 1.35 mPa.s and 1.23 mPa.s after its preparation. As can be understood from these results, the viscosity of the solution is controlled by ratio of the Cu. The solutions containing different Cu concentration usually show a more complex behavior of their viscosity, gel point, shear stress, viscous and elastic modulus. An important feature is that the rheological properties of precursor solutions directly influence the thickness of sol-gel films and higher viscosities results in higher film thickness as explained elsewhere [28]. The significant results of our study are that shear stress, viscous and elastic moduli of the solutions possess parallel values to viscosity (see

Table 2 for details). These results were measured depending on time to find gel point of the solutions. The measured gel points of ZnO-0, 5, 10 and 15% CuO-Al$_2$O$_3$ solutions were determined as 4000, 3500, 3000 and 2500 sec, respectively. To investigate in details why gel point changes as a function of temperature, rheological properties were also scrutinized at 30°C, 40°C and 50°C. Roughly speaking, the gel points of the gel points of the solutions decreased depending on increased temperature as expected. The reason of this behavior is because of evaporation of the solvent in the solutions. When the solvent evaporates from the solutions, the viscosity increases and gradually the gel point decreases due to this reality. Not only gel point is our purpose to find in this case but also viscosity is to determine inasmuch as there is a strong correlation between both. As shown from Table 2, upon increasing Cu concentration in the solution, the viscosity is slightly changed and thus also other rheological properties such as shear stress, viscous and elastic moduli.

3.2. Film Characterization

3.2.1. DTA-TG Analysis

Thermal behavior of Zn, Cu and Al based powders dried at 150°C for 1 h in air is depicted in Fig. 4. DTA-TG analysis of the Zn, Cu and Al based powder materials before removing template was conducted from 25 to 600°C with a heating rate 10°C/min to examine the heat temperatures of the template including drying/combustion, heat treatment/oxidation and annealing.

DTA curve revealed that endothermic and exothermic reactions became at temperatures between 25°C and 600°C (see Fig. 4a). As has been previously commented elsewhere [29, 30], it was due to the fact that physical water and solvent in the gel evaporated and carbon based materials coming from precursors, solvent and chelating agent burnt out. The first thermal phenomenon was occurred in the temperature range of 75 and 120°C on account of solvent removal. At these temperatures, the endothermic reaction is mostly owing to evaporation of volatile organic components. The formed entalphies of ZnO-CuO-Al$_2$O$_3$ xerogels having 0, 5, 10 and 15% CuO content during solvent removal were determined as 767 J/g, 691 J/g, 635 J/g and 194 J/g, respectively. The second phenomenon was combustion of OR groups at temperatures between 250 and 410°C. A large great exothermic peak was determined at this temperature range because of combustion of carbon based materials. On the other hand, the thermal effect in these temperature ranges is assigned to burning out organic residue resulted from the complex decomposition. It is believed that evaporation of chloride entrapped in the xerogels, coming from CuCl$_2$ and AlCl$_3$.H$_2$O precursors, occurred as well as combustion of organic materials. These results are greatly in accordance with literature [12]. The maximum temperatures of the combustion peaks were 350°C, 365°C, 370°C and 375°C for ZnO-CuO-Al$_2$O$_3$ xerogels having 0, 5, 10 and 15% CuO, respectively. It is evidence that combustion temperature increases as CuO content increases in the xerogels. The formed entalphies of ZnO-CuO-Al$_2$O$_3$ xerogels having 0, 5, 10 and 15% CuO content during combustion process were found to be 61 J/g, 506 J/g, 121 J/g and 937 J/g, respectively. The last stage was the formation of ceramic oxides between 420 and 600°C, which is in good agreement with the mentioned temperatures in the literature [29,30].

(a)

(b)
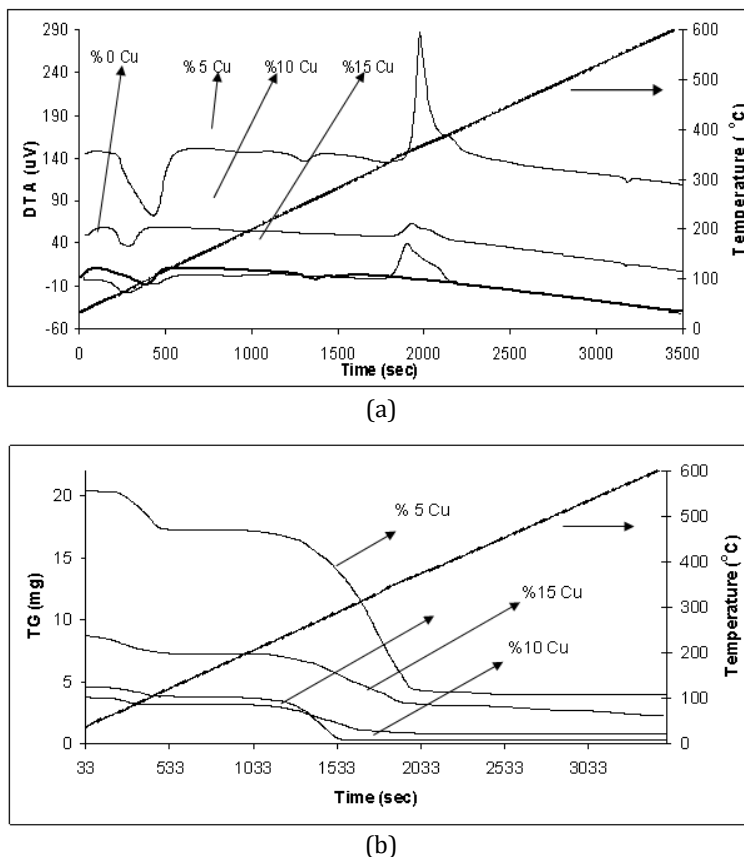
Fig. 4 (a) DTA and (b) TG curves of ZnO-0, 5, 10 and 15% CuO-1% Al_2O_3 xerogels which dried at 150 oC for 30 min in air

The TGA curve (see Fig. 4b), illustrated in the present case for ZnO-CuO-Al_2O_3 xerogel powders having 0, 5, 10 and 15% CuO, show weight losses of 94%, 81%, 78% and 74% for temperatures from 25°C up to 600°C. In this range of the thermal treatment, the weight decrease is due to solvent removal and combustion of carbon-based materials. As can be seen in TG curve, the largest weight lost is occurred in combustion of carbon based materials. The slope of TG curve is quickly decreased when carbon based materials are burnt out. Variation in the entalphies and weight losses are because the amounts of the xerogels which we used in DTA-TG experiments are different from each other. No needless to say, this amount influences only entalphies and weight losses of the materials. There is no any effect to maximum peak temperatures of combustion and oxidation due to the fact they are specific properties of materials. As can be obviously seen in these results, temperatures of combustion and oxidation depend on material type which is different. Based upon these results, we consider that the annealing temperature (600°C) can completely remove all templates from Zn, Cu and Al networks and oxide crystalline structure is completely formed at this temperature.

3.2.2. FTIR Analysis

Fig. 5 indicates the FTIR absorbance spectra of Zn, Cu and Al based powders which were dried 25°C, 100°C, 300°C, 500°C and 600°C for 30 min in air. FTIR data are in accordance

with DTA-TG and XRD results. The bands at 3200 and 4000 cm^{-1} are due to O-H species in the Zn, Cu and Al -based xerogel which was heat treated at 25°C and 300°C, respectively and those at 2800 cm^{-1} are due to C-H stretching frequencies. To illustrate, the presence of CH_2 and CH_3 organic groups was monitored through their vibrational modes occurring in the 2400–2900 cm^{-1} range. The band seen in approximately 1600 cm^{-1} is due to C=O arising due to bridging type metal-acetate bonding (M-OCOO-M). The spectra of the samples which were heat treated at 25°C, 100°C and 300°C were nearly similar. However, the OH band has shifted slightly towards lower frequencies (Fig. 5). Upon increasing heat treatment temperature from 25°C to 600°C, the frequencies of O-H, C=O and M-OCOO-M bands decreased and progressively disappeared at around 500°C. Therefore, around the transition temperature (~500°C), the changes are very fast and above 450°C no signals of O-H, C=O and M-OCOO-M bands are found. For instance, the spectrum of ZnO-CuO-Al$_2$O$_3$ precursor film annealed at 500°C and 600°C which shows an absence of absorption bands corresponding to organics and hydroxyls indicating complete removal of organics and hydroxyls. The films in this region are of good crystalline and oxidation qualities. The common features that appear below 600 cm^{-1} corresponds to the stretching vibrations of Zn=O, Cu=O and Al=O and also to the contributions of Zn-O, Cu-O and Al-O bonds. In the spectrum of 500°C and 600°C, the band at ≈ 450 cm^{-1} may be assigned to the vibration of ZnO, CuO and Al$_2$O$_3$ bands appear at high temperatures [31]. The intensities of the bands increased with increasing temperature because of oxide formation. This was confirmed by XRD as explained in structural analysis later. Likewise, oxide content can be monitored as a function of heat treatment temperature, changing from 25°C from 600°C. The oxide formation progressively appears with increasing heat treatment temperature.
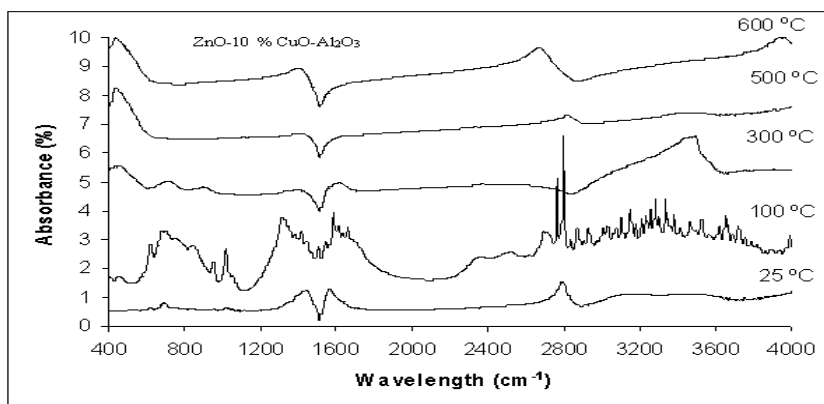

Fig. 5 FTIR absorbance spectra of Zn, Cu and Al based powders heat treated at different temperatures for 30 min in air

3.2.3. Structural Analysis

Fig. 6 depicts XRD patterns of ZnO and ZnO-CuO-Al$_2$O$_3$ thin films on glass substrate. ZnO and CuO phases were obtained after annealing process performed at 600°C for 30 min in air. Most peaks are identified as the diffraction lines of ZnO species and only a small peak is assigned to CuO. This is evidence from Fig. 6 that the intensity of CuO peaks increased when CuO content in the composite films are increased. Al$_2$O$_3$ phase was not found from XRD results due to the fact that the composites films had 1% Al$_2$O$_3$ content. Similar results were reported in Ref. [32]. The XRD pattern clearly showed the polycrystalline nature of the ZnO-CuO-Al$_2$O$_3$ composite films, whose random orientations were obtained. A very broad peak around 2θ = 22° is caused by the glass substrate [3]. A small and sharp

peak appears around $2\theta = 34°$ for 1 dipping corresponding to the diffraction by a (002) plane of ZnO crystal and other smaller diffractions of ZnO crystals occur in greater degrees of 2θ. The c-axis (002) can be produced with increasing annealing temperature [1]. In addition to annealing temperature, the multilayered sol-gel films are considered to disturb the overall growth of the films with c-axis orientation [33].
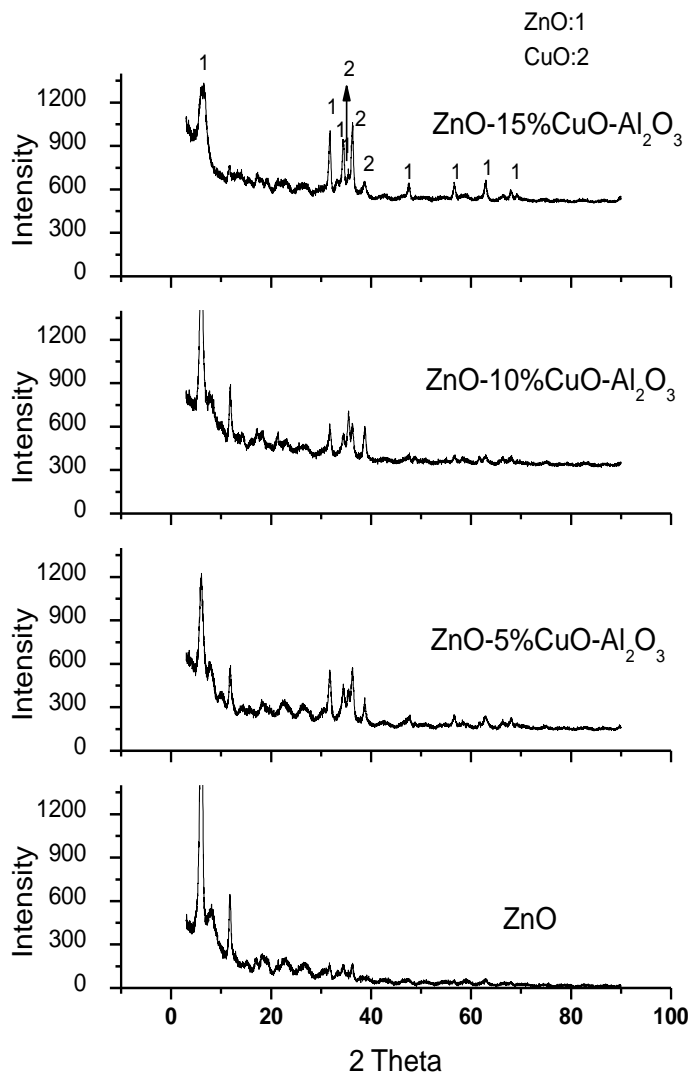
Fig. 6 XRD results of ZnO, ZnO-5% CuO-1% Al_2O_3, ZnO-10% CuO-1% Al_2O_3 and ZnO-15% CuO-1% Al_2O_3 films prepared on glass substrates by sol-gel technique

3.2.4. Surface Features

3.2.4.1. SEM-EDS

Fig. 7 shows surface morphologies of ZnO and ZnO-CuO-Al_2O_3 films prepared by sol-gel dip-coating process. SEM photographs depict a little difference in morphology among the three film surfaces. From these micrographs one can see the total coverage of the

substrate with the clusters of ZnO-CuO-Al$_2$O$_3$. During deposition of ZnO based films by sol-gel dipping technique, the growth has taken place by nucleation and coalescence processes as reported by V.R. Shinde et al. [34]. Randomly distributed (002) oriented nuclei may have first formed and these nuclei have grown to form observable islands. As islands increase their size by further deposition and come closer to each other, the larger ones appeared to grow by coalescence of smaller one. Flattening of islands to give increased surface coverage of clusters follows this step. The shape of the oxide particles obtained via sol–gel technique is modeled to depend on the growth mechanisms. The growth of the oxide particles occurs either by mononuclear or polynuclear growth mechanism. In mononuclear growth mechanism, the particles grow by formation of successive layers. During the operation of this growth mechanism, the first step is created on the nucleated particle surface. There is enough time to complete a layer before a new begins. Growth proceeds via 'a layer-by-layer' mechanism, and these layers correspond to densest packing of polynuclear complexes. The particle surfaces are locally smooth at the molecular level but faceted at the microscopic scale. These particles take well defined shapes, corresponding to particular crystal structures. In the mononuclear growth region, the particle growth rate is proportional to the particle surface area, $dr/dt = k_m r^2$. As the particles grow initially by a mononuclear growth mechanism, the surface area of the layer increases and the growth mechanism progressively changes to a polynuclear growth mechanism [13].

As shown in Fig. 7a, some micropores and pits are distributed in the microstructure of ZnO films. This can be attributed to the osmotic shrinkage mechanism in drying process. Furthermore, these inhomogeneties might be occurred during deposition through which the gases have escaped due to the compact nature of ZnO clusters [13,34]. Surface morphology of ZnO-CuO-Al$_2$O$_3$ films has drastically changed as shown in Figs. 7b, 7c and 7d. Cu and Al atoms may have disturbed the growth process resulting into formation of nanosize grains. Depending on CuO content, smooth surfaces formed all over the surfaces. In Figs. 7c and 7d, amounts of micro-pores decrease by adding CuO and Al$_2$O$_3$. All pores and pits disappear and a dense microstructure is obtained by adding %15 CuO as seen in Fig. 7d. Actually, gas sensors are essentially thin discs of porous material that change in resistivity when exposed to atmospheres containing certain gases [6]. Furthermore, Fig. 7e demonstrates EDS result of ZnO-CuO-Al$_2$O$_3$ film on glass substrate. It is clear from this figure that Zn, Cu and Al elements are present in the films. EDS result in Fig. 7e was taken from Fig. 7d which shows SEM micrograph of the film. The intensity of Zn peak is higher than that of other elements. Cu peak overlaps Zn one as shown in Fig. 7e Al peak is very low because it has 1% Al$_2$O$_3$ in the films.
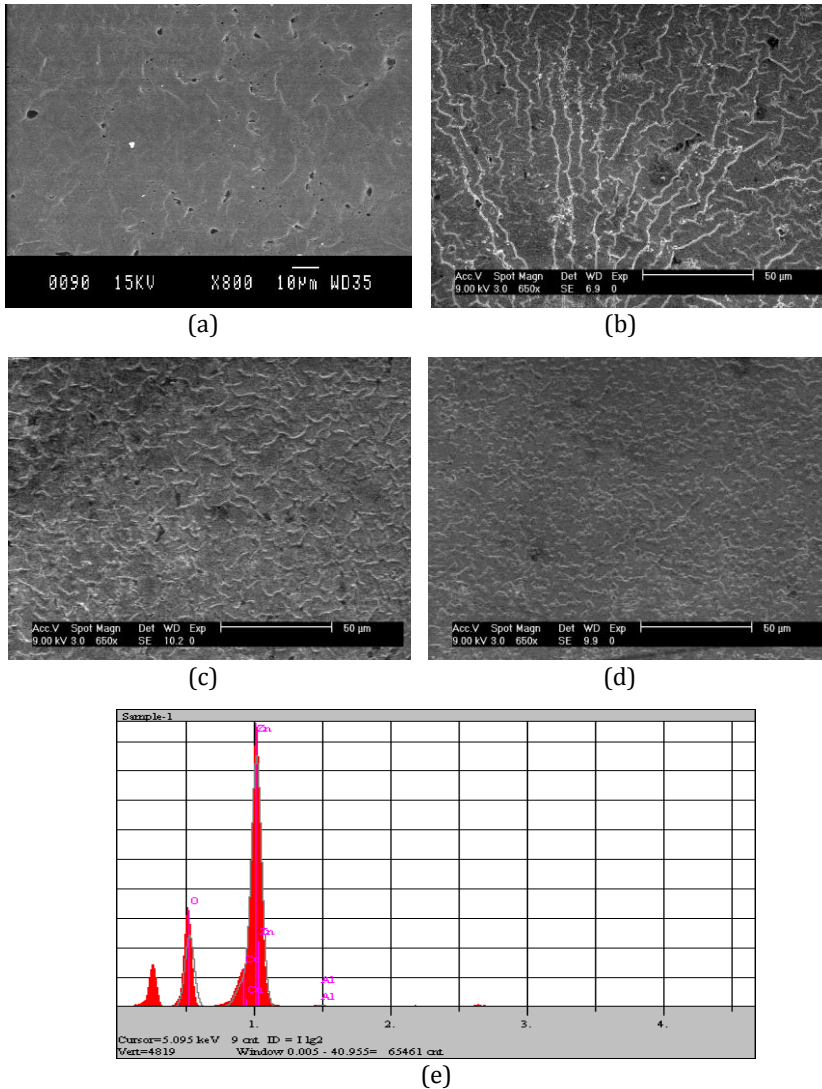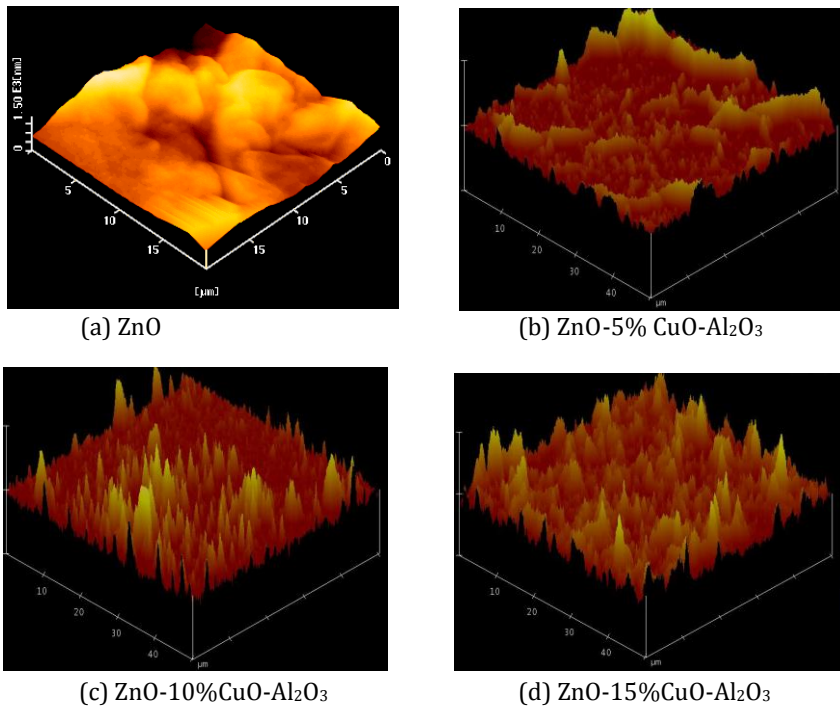
Fig. 7 SEM micrographs of (a) ZnO, (b) ZnO-5% CuO-1% Al_2O_3 (c) ZnO-10% CuO-1% Al_2O_3 and (d) ZnO-15% CuO-1% Al_2O_3 films on glass substrates and (e) EDS analysis of ZnO-15% CuO-1% Al_2O_3 films on glass substrates in Fig. 7d

3.2.4.2. AFM

Concerning with surface roughness and quality of the films, AFM was used to examine surface quality in details. After acquiring an AFM image, the image was subjected to a second order flattening procedure using the Autoprobe CP image processing software. This procedure removes the nonlinear background artifact introduced by the piezo scanner. Following the flattening procedure, the surface roughness was quantified using a root mean squared (RMS) roughness calculated from:

$$RMS = \sqrt{\frac{\sum_{i-1}^{N}(z_i - z_a)^2}{N-1}}$$ (6)

In this equation, z_i is the image height at pixel i, z_a is the average height and N is the number of pixels in the AFM image. The RMS roughness values calculated from the AFM images of a given film varied slightly from tip to tip. Because the AFM tips inevitably break with repeated use, recording all of the AFM data in this study with a single tip was not possible. To address this problem, care was taken to ensure that all the data in a given figure was measured using the same AFM tip. Consequently, although the differences are slight, the RMS roughness values may not be directly comparable from one figure to another. The AFM scan size may affect the RMS roughness values [35]. This behavior arises because longer wavelength topography components are sampled with increasing scan size. To quantify this effect, AFM images were recorded from ZnO-based films at various scan sizes ranging from 10 nm to 4 μm. The RMS roughness values calculated from these images increased sharply with scan size between 20 μm and 50 μm. AFM images of ZnO and ZnO-CuO-Al$_2$O$_3$ films on glass substrates are shown in Fig. 8 is indicative of the grain growth in the direction perpendicular to the substrate surface. Surface roughnesses of ZnO and ZnO-CuO-Al$_2$O$_3$ films were in the range of 90 to 200 nm.

(a) ZnO

(b) ZnO-5% CuO-Al$_2$O$_3$

(c) ZnO-10%CuO-Al$_2$O$_3$

(d) ZnO-15%CuO-Al$_2$O$_3$

Fig. 8 AFM micrographs of (a) ZnO, (b) ZnO-5%CuO-1%Al$_2$O$_3$, (c) ZnO-10%CuO-1%Al$_2$O$_3$ and (d) ZnO-15%CuO-1%Al$_2$O$_3$ films on glass substrates

The important feature here is that the surface quality improved by decreasing surface roughness when increasing CuO content in the films. It can be numerically stated that the surface roughness values for the ZnO-CuO-Al$_2$O$_3$ solutions including 0, 5, 10 and 15% CuO were determined to be 200 nm, 160 nm, 120 nm and 90 nm, respectively. Because a rather high thickness of the film was obtained by six layers deposition, but in the same

time the average roughness of the film is rather high. The relative high value of the roughness can be assigned to the agglomeration phenomena during the thermal processes of the deposited layer on glass substrates.

3.2.5. Adhesion

In the scratch testing of thin coatings, the usual procedure is to move the scratch tip across the coated surface under an increasing load until, at a certain load referred to as the critical load a well-defined failure event occurs. In this system, measurement of the load–displacement characteristics provides another simple means to determine the critical load, since the failure or detachment of the coating usually results in an abrupt change in the load–displacement characteristics. The failure mode and the value of the critical load depend on the various parameters, namely, the properties of the substrate, the coating, and the coating–substrate interface, the coating thickness, the shape of the scratch tip, the loading rate, and the friction between the scratch tip and the coating surface [35].

As we explained about details of adhesion procedure of sol-gel dipping coatings elsewhere [36] and briefly summarized here, the objective of scratch test is to evaluate the adhesion between coating and substrate. In the test, increasing normal load is applied to the diamond stylus. Simultaneously, diamond stylus is scratched over the surface of the coating with a constant speed. The load at which failure occurs on the coating is defined as critical load. The test load versus cartridge output (%) curves for ZnO and ZnO-CuO-Al_2O_3 films on glass substrates were given in Fig. 9.
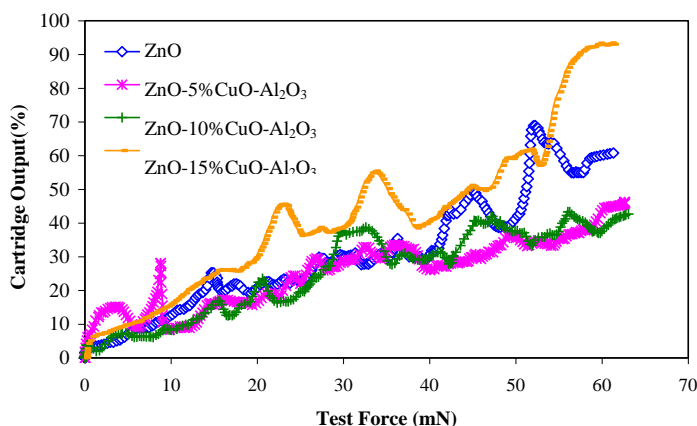

Fig. 9 Adhesion properties of ZnO-0, 5, 10 and 15% CuO-1% Al_2O_3 films on glass substrate

During the scratch test, with increasing applied load, friction of the stylus becomes large; therefore delay in movement of the stylus from that of the cartridge body also becomes large. This delay is given as a cartridge output. Critical load values of ZnO and ZnO-CuO-Al_2O_3 films were found from Fig. 9, when sudden increase takes place at the cartridge output. The critical load values of the ZnO-CuO-Al_2O_3 films prepared from the solutions including 0, 5, 10 and 15% CuO content were found to be 17, 22, 28 and 36 mN, respectively. This is due to the fact that residual stresses which cause mechanical failures increase with increasing film thickness of ZnO-CuO-Al_2O_3 films on glass substrate. Therefore, the films prepared from 15% CuO have better adhesion strength to the glass

substrate among other coatings. As can be seen from these results, critical load values of the coatings increase with the increasing amount of the methanol. Generally speaking, improvement in adhesion properties was determined depending on coating thickness. Adhesion is directly related to wettability, solution viscosity and coating thickness.

3.2.6. Optical Properties

The optical properties of these films were investigated. Table 3 shows refractive index, porosity, film thickness and band gap values of the films. It is clear from Table 3 that there are strong relationships among refractive indexes, porosity and film thickness as demonstrated in ITO films by H.R. Fallah et al. [37]. The refractive indexes (n) of porosity of ZnO-CuO-Al$_2$O$_3$ films are listed as a function of CuO content. Fig. 10 shows the porosity values obtained from Eqs. 1, 2 and 3 for ZnO-0, 5, 8 and 12% CuO-Al$_2$O$_3$ films as a function of refractive index, assuming that n_d=1.95, 1.93, 1.92 and 1.90 for these specific materials with pore-free, respectively [34,37,38].
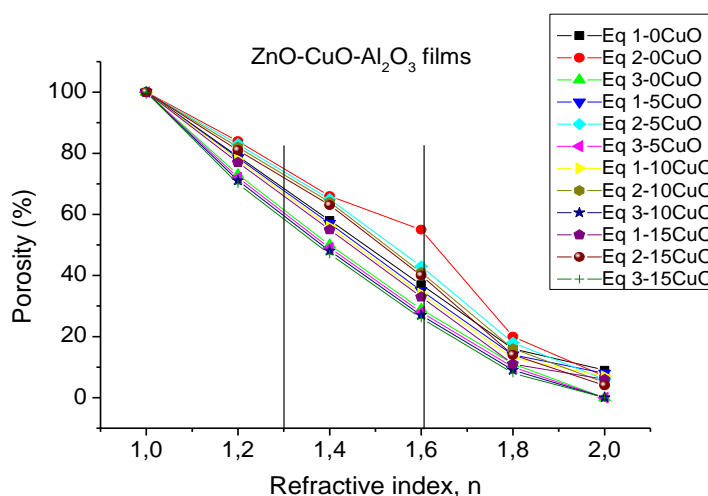
Fig. 10 Variations of porosity as a function of refractive index for ZnO, ZnO-0, 5, 10 and 15%CuO-1%Al$_2$O$_3$ films on glass substrates

Deposited films are assumed to be homogenous in the calculations. As one can see, porosity values vary considerably from one expression to another. It should be mentioned that refractive indices of ZnO based sol–gel coatings usually lie within the interval 1.20–1.70 in which the differences are especially pronounced (see Fig. 10 for details). Therefore questions arise concerning the validity of these expressions. But yet, the porosities of the coatings can be estimated to be in the range of 20 and 60%. Besides, while pure ZnO films has a high porosity, the porosity values of ZnO-5, 10 and 15% CuO-Al$_2$O$_3$ films decrease as a function of CuO content. As indicated in effect on phase structure and microstructure of CuO in the films before, it can be stated that reasonable porosity values were found because CuO decrease porosity of the coatings. These films, however, have a larger porosity. It would be expected that porosity in the films would increase the scattering of carriers, reducing their mobility. This is an apparent contradictory result. It would be stressed that Eqs. 1, 2 and 3 are well satisfied for fairly thick films, but that for thin films the porosity values will be overestimated [37]. For obtaining trustworthy porosity values for ZnO-0, 5, 10 and 15% CuO-Al$_2$O$_3$ films it is necessary to use other techniques. In addition, the film thicknesses for ZnO-0, 5, 10 and

15% CuO-Al$_2$O$_3$ were measured as 852 nm, 478 nm, 518 nm and 695 nm using optical method respectively. The thickness of the film can be modified and the roughness could be improved by appropriate changes of the preparation conditions of the solutions and of the deposition procedure.

Table 3
Refractive index, porosity, film thickness and band gap values of the films

Films	Refractive index	Porosity (%)	Film thickness (nm)	Energy gap (eV)
ZnO	1.2985	60	852	3.18
ZnO-5%CuO-Al$_2$O$_3$	1.3097	55	478	3.17
ZnO-10%CuO-Al$_2$O$_3$	1.5586	27	518	3.16
ZnO-15%CuO-Al$_2$O$_3$	1.6081	20	695	3.15

The optical absorption of ZnO based semiconducting films was given in Fig. 11. Spectra of the composite films was analyzed by plotting $(\alpha h\nu)^2$ versus $h\nu$ curve based on the relationship $\alpha h\nu = A(h\nu - Eg)^{1/2}$, where is a constant and n depends on the nature of the the transition (n=1 for direct allowed transition). These curves clearly show distinct straight lines, and from the intercept of the straight lines on the energy ($h\nu$) axis the band-gap is estimated [6]. Thus the optical direct band gap energies obtained are about 3.18, 3.17, 3.16 and 3.15 eV for ZnO-CuO-Al$_2$O$_3$ films including 0, 5, 10 and 15% CuO content, which notably is in good agreement with the value of ZnO obtained by Y. Natsude et al. [1]. It is also reasonable that the band gap energies decrease as a function of CuO content because CuO exhibits semiconducting behavior.
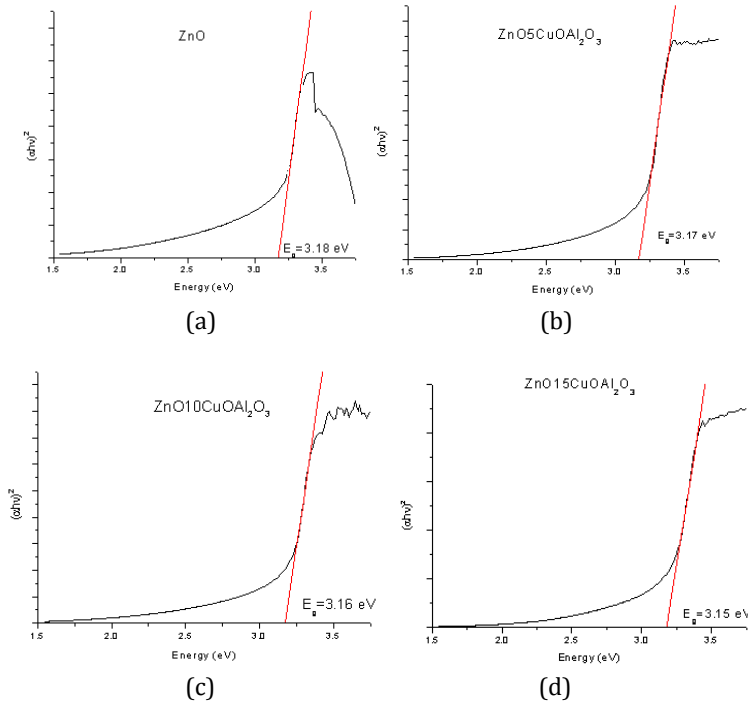
Fig. 11 Optical direct band gap energies of a) ZnO, (b) ZnO-5% CuO-1% Al$_2$O$_3$ (c) ZnO-10% CuO-1% Al$_2$O$_3$ and (d) ZnO-15% CuO-1% Al$_2$O$_3$ films on glass substrates

Fig. 12 depicts optical transmission spectra in the wavelength (λ) range 300-800 nm for ZnO-CuO-Al$_2$O$_3$ films which include 0, 5, 10 and 15% CuO content, formed by sol-gel dip-coating at 600°C for 1 hour in air. The optical spectra for all films give the transparency in the visible range 320 to 380 nm. ZnO film was found to be transparent in the visible range with range a sharp absorption edge at wavelength of about 380 nm, which is very close to the intrinsic band-gap of ZnO (3.19 eV). This result is good agreement with M. Ohyama et al. [3]. Nevertheless, in ZnO-CuO-Al$_2$O$_3$ films having 0, 5, 10 and 15% CuO, transparency in the visible range with a wide absorption edge at wavelength of 320-380 nm. The ZnO film shows the transmittance of the order of 44% while that of ZnO-CuO-Al$_2$O$_3$ films was of the order of 55%. It is noticed that the ZnO film has higher absorbance in visible range of spectrum. The absorbance has increased after addition of CuO and Al$_2$O$_3$. This behavior may be due to introduction of the Cu and Al defect states within forbidden band.
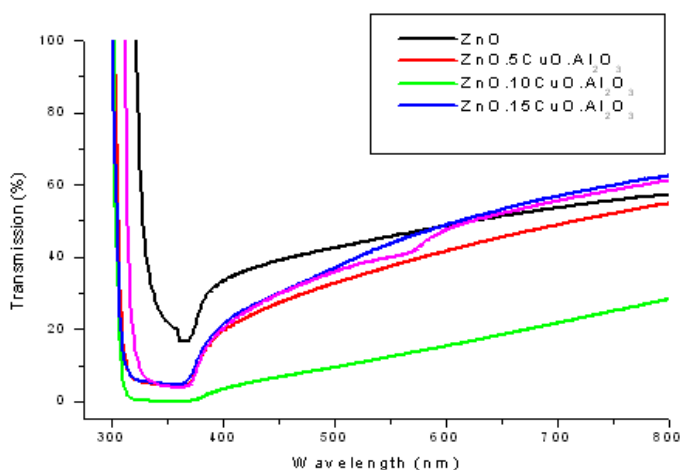
Fig. 12 Transmission vs. wavelength curves for ZnO based composite films on glass substrates

4. Summary, Conclusions and Outlook

ZnO and ZnO-CuO-Al$_2$O$_3$ semiconducting thin films were successfully fabricated on glass substrates using solutions prepared from Zn, Cu and Al based precursors, methanol and acetic acid by sol-gel dip-coating method for gas sensor applications. Turbidity values of the ZnO-CuO-Al$_2$O$_3$ solutions including 0, 5, 10 and 15% CuO were respectively measured as 33.90, 33.70, 34.80 and 33.80 ntu, indicating that powder based precursors are dissolved in the solutions. The pH values of the solutions were found to be in the range of 4.28 and 4.59. The pH values decreased depending on CuCl$_2$ concentration because Cl content, which comes from Cu- and Al-based chlorides, increased in the solutions. The contact angles for the ZnO-CuO-Al$_2$O$_3$ solutions including 0, 5, 10 and 15% CuO were found to 18.01°, 16.01°, 17.02° and 21.38°, respectively. The relative viscosity values of the obtained ZnO-CuO-Al$_2$O$_3$ solutions having 0, 5, 10 and 15% CuO were found to be 1.21 mPa.s, 1.42 mPa.s, 1.35 mPa.s and 1.23 mPa.s after its preparation. The solutions containing different Cu concentration usually show a more complex behavior of their viscosity, gel point, shear stress, viscous and elastic modulus. The rheological properties of precursor solutions directly influence the thickness of sol-gel films and higher viscosities results in higher film thickness. The measured gel points of ZnO-0, 5, 10 and 15% CuO-Al$_2$O$_3$ solutions were approximately determined as 4000, 3500, 3000 and 2500

sec, respectively. When increasing Cu concentration in the solution, the viscosity is slightly changed and thus also other rheological properties such as shear stress, viscous and elastic moduli.

DTA curve revealed that endothermic and exothermic reactions became at temperatures between 25°C and 600°C. The formation of ceramic oxides was occurred at temperatures between 420 and 600°C. The annealing temperature (600°C) can completely remove all templates from Zn, Cu and Al networks and oxide crystalline structure is completely formed at this temperature. The spectrum of ZnO-CuO-Al_2O_3 precursor film annealed at 500°C and 600°C which shows an absence of absorption bands corresponding to organics and hydroxyls indicating complete removal of organics and hydroxyls. In the spectrum of 500°C and 600°C, the band at ≈ 450 cm^{-1} may be assigned to the vibration of ZnO, CuO and Al_2O_3 bands appear at high temperatures. The intensities of the bands increased with increasing temperature because of oxide formation. XRD supported DTA-TG and FTIR results, showing that ZnO and CuO phases were obtained after annealing process. A small and sharp peak appears around $2\theta = 34°$ for 1 dipping corresponding to the diffraction by a (002) plane of ZnO crystal and other smaller diffractions of ZnO crystals occur in greater degrees of 2θ. The c-axis (002) can be produced with increasing annealing temperature. Randomly distributed (002) oriented nuclei may have first formed and these nuclei have grown to form observable islands. A good inter-grain connection is developed by increasing the amount of CuO in structure and poreless coating was achieved by adding %15 CuO. Cu and Al atoms may have disturbed the growth process resulting into formation of nanosize grains. Depending on CuO content, smooth surfaces formed all over the surfaces. It is clear that Zn, Cu and Al elements are present in the films. Al peak is very low because it has 1% Al_2O_3 in the films. AFM results revealed that surface roughnesses of ZnO and ZnO-CuO-Al_2O_3 films were in the range of 90 to 200 nm. The surface quality improved by decreasing surface roughness when increasing CuO content in the films. The critical load values of the ZnO-CuO-Al_2O_3 films prepared from the solutions including 0, 5, 10 and 15% CuO content were found to be 17, 22, 28 and 36 mN, respectively. The films prepared from 15% CuO have better adhesion strength to the glass substrate among other coatings.

It is clear that there are strong relationships among refractive index, porosity and film thickness. It should be mentioned that refractive indices of ZnO based sol–gel coatings usually lie within the interval 1.3–1. While pure ZnO films has a high porosity, the porosity values of ZnO-5, 10 and 15% CuO-Al_2O_3 films decrease as a function of CuO content. It can be stated that reasonable porosity values were found because CuO decrease porosity of the coatings. The film thicknesses for ZnO-0, 5, 10 and 15% CuO-Al_2O_3 were measured as 852 nm, 478 nm, 518 nm and 695 nm using optical method respectively. The optical direct band gap energies of ZnO-CuO-Al_2O_3 films including 0, 5, 10 and 15% CuO were 3.18, 3.17, 3.16 and 3.15 eV, respectively. It is also reasonable that the band gap energies decrease as a function of CuO content because CuO exhibits semiconducting behavior. Also, the optical spectra for all films give the transparency in the visible range of 320 to 380 nm. The ZnO film shows the transmittance of the order of 44% while that of ZnO-CuO-Al_2O_3 films was of the order of 55%.

Acknowledgements

References

1. Natsume Y and Sakata H. Zinc oxide films prepared by sol-gel spin coatings. Thin Solid Films, 2000; 372: 30 – 36.
2. Chang JF, Kuo HH, Leu IC and Hon MH. The effects of thickness and operation temperature on ZnO:Al thin film CO gas sensor. Sensors and Actuators B, 2002; 84: 258 – 264.
3. Ohyama M, Kozuka H and Yoko T. Sol-gel preparation of ZnO films with extremely preferred orientation along (002) plane from zinc acetate solution. Thin Solid Films, 1997, 306: 78 – 85.
4. Moulson AJ and Herbert JM. Electroceramics, Charpman & Hall, 1990, p. 163.
5. Bae HY, Choi GM. Electrical and reducing gas sensing properties of ZnO and ZnO - CuO thin films fabricated by spin coating method. Sensors and Actuators B, 1999; 55: 47 – 54.
6. Ray SC. Preparation of copper oxide thin film by the sol-gel-like dip technique and study of their structural and optical properties. Solar Energy Materials & Solar Cells, 2001; 68: 307 – 312.
7. Shi C, Fu Z, Guo C, Ye X, Wei Y, Deng J, Shi J and Zhang G. UV luminescence and spectral properties of ZnO films deposited on Si substrates. J. Electron Spectroscopy and Related Phenomena, 1999; 101 – 103: 629 – 632.
8. Kamalasanan MN and Chandra S. Sol-gel of ZnO thin films. Thin Solid Film, 1996; 288: 112 – 115.
9. Fujihara S, Sasaki C and Kimura T. Crystallization behavior and origine of c-axis orientation in sol-gel derived ZnO: Li thin films on glass substrates. Applied Surface Science, 2001; 180: 341 – 350.
10. Purica M, Budianu E, Rusu E, Danila M and Gavrila R. Optical and structural investigation of ZnO thin films prepared by chemical vapor deposition (CVD). Thin Solid Film, 2002; 403 – 40: 485 – 488.
11. Bandyopadhyay S, Paul GK, Roy R, Sen SK and Sen S. Study of structural and electrical properties of grain-boundary modified ZnO films prepared by sol–gel technique. Materials Chemistry and Physics, 2002; 74: 83 – 91.
12. Pierre AC. Introduction to sol-gel processing. Kluwer Academic Publishers, 1998: 237.
13. Liu YL, Liu YC, Liu YX, Shen DZ, Lu YM, Zhang JY and Fan XW. Structural and optical properties of nanocrystalline ZnO films grown by cathodic electrodeposition on Si substrates. Physica B: Condensed Matter, 2002; 322: 31 – 36.
14. Bhuiyan MS, Paranthaman M and Salama K. Solution-derived textured oxide thin films-a review. Supercond. Sci. Technol., 2006; 19: R1 – R21.
15. Diaz-Parralejo A, Caruso R, Ortiz AL and Guiberteau F. Densification and porosity evaluation of ZrO_2–3 mol% Y_2O_3 sol–gel thin films. Thin Solid Films, 2004; 458: 92 – 97.
16. Ech-chamikh E, Essafti A, Azizan M and Ijdiyaou Y. XPS study of amorphous carbon nitride (a-C:N) thin films deposited by reactive RF sputtering. Solar Energy Materials and Solar Cells, 2006; 90: 1424 – 1428.
17. Wilde FD and Gibs J. Turbidity. Geological Survey TWRI Book, 9: 1 – 30.
18. Xu Y and Li L. Thermoreversible and salt-sensitive turbidity of methylcellulose in aqueous solution. Polymer 46, 2005; 7410 – 7417.
19. Jerónimo PCA, Araújo AN, Conceição M and Montenegro BSM. Development of a sol–gel optical sensor for analysis of zinc in pharmaceuticals. Sensors and Actuators B: Chemical, 2004; 103: 169 – 177.

20. Sheffer M, Groysman A and Mandler D. Electrodeposition of sol–gel films on Al for corrosion protection. Corrosion Science, 2003; 45: 2893 – 2904.
21. Brinker CJ and Scherer GW. Sol-Gel Science: The Physics and Chemistry of Sol-Gel Processing, Academic Press, San Diego, 1990: 2, 656.
22. Pierre AC. Introduction to Sol-gel Processing, Kluwer Academic Publishers, Boston, 1998: 36.
23. Celik E, Avci E and Hascicek YS. Growth Characteristic of ZrO_2 Insulation Coatings on Ag/AgMg Sheathed Bi-2212 Superconducting Tapes. Materials Science and Engineering B, 2004; 110: 213 – 220.
24. Phonthammachai N, Rumruangwong M, Gulari E, Jamieson AM, Jitkarnka S and Wongkasemjit S. Synthesis and rheological properties of mesoporous nanocrystalline CeO_2 via sol–gel process. Colloids and Surfaces A: Physicochemical and Engineering Aspects, 2004; 247: 61 – 68.
25. Abel-Aal EA, Ismail AA, Rashad MM and El-Shall H. New approach for measuring gelation rate during synthesis of ZnO/SiO_2 gel. Journal of Non-Crystalline Solids, 2006; 352: 399 – 403.
26. Baraton MI. Synthesis, Functionalization and Surface Treatment of Nanoparticles, American Scientific Publishers, 2003: 10.
27. Rudé Payró E and Llorens Llacuna J. Rheological characterization of the gel point in sol–gel transition. Journal of Non-Crystalline Solids, 2006; 352: 2220 – 2225.
28. Knoth K, Hühne R, Oswald S, Schultz L and Holzapfel B. Highly textured $La_2Zr_2O_7$ buffer layers for YBCO coated conductors prepared by chemical solution deposition. Supercond. Sci. Technol., 2005; 18: 334 – 339.
29. Celik E, Yildiz AY, Tanoglu M, Ak Azem NF, Toparli M, Emrullahoglu OF and Ozdemir I. Preparation and Characterization of Fe_2O_3-TiO_2 Thin Films on Glass Substrate for Photocatalytic Applications. Materials Science and Engineering B, 2006; 129: 1993 – 1997.
30. Celik E, Gokcen Z, Ak Azem NF, Tanoglu M and Emrullahoglu OF. Processing, characterization and photocatalytic properties of Cu doped TiO_2 thin films on glass substrate by sol–gel technique. Materials Science and Engineering: B, 2006; 132: 258 – 265.
31. Ning W, Shen H and Liu H. Study of the effect preparation method on CuO-ZnO-Al_2O_3 catalyst. Applied Catalysis A: General, 2001; 211: 153 – 157.
32. Sha ZD, Wang J, Chen ZC, Chen AJ, Zhou ZY, Wu XM and Zhuge LJ. Initial study on the structure and optical properties of ZnO film on Si (111) substrate with a SiC buffer layer. Physica E: Low-dimensional Systems and Nanostructures, 2006; 33: 263 – 267.
33. Tahar RBH. Structural and electrical properties of aluminum-doped zinc oxide films by sol-gel process. J. of the European Ceramic Society, 2005; 25: 3301 – 3306.
34. Shinde VR, Gujar TP, Lokhande CD, Mane RS, Han S-H. Mn doped and undoped ZnO films: A comparative structural, optical and electrical properties study. Materials Chemistry and Physics, 2006; 96: 326 – 330.
35. Malzbender J, den Toonder JMJ, Balkenende AR and de With G. Measuring mechanical properties of coatings: a methodology applied to nano-particle-filled sol–gel coatings on glass. Materials Science and Engineering: R: Reports, 2002; 36: 47 – 103.
36. Celik E, Keskin I, Kayatekin I, Ak Azem F and Özkan E. Al_2O_3–TiO_2 thin films on glass substrate by sol–gel technique. Materials Characterization, 2007; 58: 349 – 357.

37. Fallah HR, Ghasemi M, Hassanzadeh A and Steki H. The effect of deposition rate on electrical, optical and structural properties of tin-doped ITO films on glass at low substrate temperature. Physica B, 2006; 373: 274 – 279.
38. Papadimitropoulos G, Vourdas N, Em Vamvakas V and Davazoglou D. Optical and structural properties of copper oxide thin films grown by oxidation of metal layers. Thin Solid Films, 2006; 515: 2428 – 2432.